Removal of Probe Liftoff Effects on Crack Detection and Sizing in Metals by the AC Field Measurement Technique

Reza K. Amineh[1], Maryam Ravan[2], S. H. Hesamedin Sadeghi[3], and Rouzbeh Moini[3]

[1]Department of Electrical and Computer Engineering, McMaster University, Hamilton, ON L8S 4K1, Canada
[2]Department of Electrical and Computer Engineering, University of Toronto, Toronto, ON M5S 1A4, Canada
[3]Department of Electrical Engineering, Amirkabir University of Technology, Tehran, Iran

In the alternative current field measurement (ACFM) technique, the nonzero value of liftoff distance for the magnetic sensor acts as a low-pass filter on surface crack signals, causing errors in crack detection and sizing. We present a blind deconvolution algorithm for liftoff evaluation and surface crack signal restoration. The algorithm employs the available closed-form expressions for the distribution of electromagnetic fields at the metal surface in the vicinity of a crack. To examine the accuracy of the algorithm, we use the original and the restored signals for crack sizing by a wavelet network inversion method. We present simulated and experimental results to demonstrate the role of the proposed algorithm in improving the inversion process.

***Index Terms*—AC field measurement, crack sizing, deconvolution, liftoff, nondestructive evaluation.**

I. INTRODUCTION

THE alternative current field measurement (ACFM) is a nondestructive evaluation (NDE) technique that offers a simple and accurate means for detection and sizing surface-breaking cracks in metals [1]–[6]. The technique uses a group of current-carrying wires of sufficiently high frequency to induce eddy currents in the workpiece while monitoring the surface magnetic field variations with an appropriate magnetic field sensor. The interpretation of sensor output signal in the ACFM technique is based on the assumption that the sensor is placed very close to the metal surface and is capable of performing point measurements of the surface magnetic field [7].

In practice, the surface of the work-piece may be covered with such layers of insulating materials as paint so that the close proximity of the sensor and the metal surface may not be possible. The nonzero value of liftoff distance acts as a low-pass filter and tends to smear out the variations in the ACFM crack signal, leading to significant errors in crack detection and sizing [8].

In this paper, we aim to suppress the filtering effect of sensor liftoff on ACFM crack signals by performing a deconvolution algorithm. However, the liftoff filtering function is partially known due to the uncertainty in true value of liftoff which, in turn, makes the use of a conventional deconvolution algorithm impractical. To overcome the problem, we propose a blind deconvolution algorithm for evaluation of the sensor liftoff from which the surface crack signal can be restored. As *a priori* information, the algorithm employs the available expressions for the distribution of electromagnetic fields at the metal surface in the vicinity of cracks [4], [5]. An appropriate cost function is constructed based on these expressions and is optimized to give an estimation of liftoff distance as well as the restored surface crack signal. In order to investigate the efficiency of the proposed algorithm on the accuracy of crack shape estimation, we use a wavelet network (WN) approach [7] for inverting both the original and the restored ACFM crack signals to the depth profiles of arbitrary shape cracks.

The paper is organized as follows. In Section II, the theoretical model used in the estimation of ACFM crack signal is outlined. Section III describes the proposed blind deconvolution algorithm for reducing the filtering effect of liftoff distance on the crack signal. In Section IV, the structure of the WN for estimating the crack shape is described. The validity and efficiency of the proposed algorithm are demonstrated in Section V where the results of several case studies are discussed.

II. PREDICTION OF PROBE OUTPUT

Fig. 1 shows the schematic diagram of the ACFM method. In this model, a semi-infinite metal with conductivity σ and permeability μcontains an arbitrary shape surface crack of length l along the x-axis. Crack depth is along the z-axis, which is perpendicular to the metal surface. The crack opening, g, is assumed to be much smaller than the crack depth, d, and length, l. The interrogated magnetic field is produced by a solenoid inducer carrying a sufficiently high frequency alternating current of frequency f and magnitude I_{m}, such that the current skin depth ($\delta = 1/\sqrt{\pi f \sigma \mu}$) is much smaller than the crack depth and length. With reference to Fig. 1, the solenoid consists of several turns of winding wire of rectangular cross section with dimensions w, L, and t, separated from each other by distance s. A tiny induction-coil sensor, monitors magnetic field variations around the crack at location (x_s, y_s, lo).

The solution of the problem is described elsewhere [4], [5]. Here, we briefly outline the solution procedure. Outside the crack and above the metal surface in air, the divergence-free magnetic field $\boldsymbol{H}$ is also curl-free as the conductive current is zero and the displacement current is assumed to be zero in frequencies of interest. As a result, one may derive $\boldsymbol{H}$ from a scalar magnetic potential function (i.e., $\boldsymbol{H} = -\nabla\psi$) with Laplacian

Digital Object Identifier 10.1109/TMAG.2008.923393

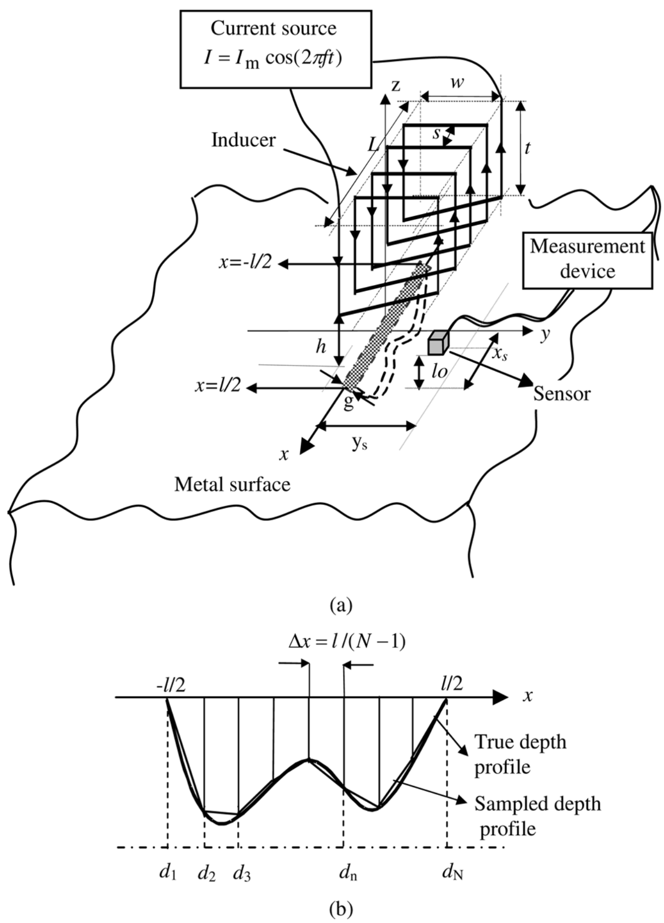

Fig. 1. Schematic diagram of the ACFM method. (a) Rectangular cross-section solenoid inducer above the surface of a conducting slab containing an arbitrary-shape surface crack. (b) Actual and discretized crack depth profiles.

distribution (i.e., $\nabla^2\psi = 0$). It can be shown that the two-dimensional (2-D) Fourier transform (FT) of ψ can be expressed as follows [4]:

$$\begin{aligned}\tilde{\tilde{\psi}}(\alpha,\beta,lo) &= \tilde{\tilde{\psi}}_{\rm i}(\alpha,\beta lo)e^{\gamma lo} + \left(\frac{1-\dfrac{\mu_{\rm r}}{k}\gamma}{1+\dfrac{\mu_{\rm r}}{k}\gamma}\right)\tilde{\tilde{\psi}}_{\rm i}(\alpha,\beta,lo)e^{-\gamma lo}\\ &\quad + \left(\frac{\dfrac{2\mu_{\rm r}}{k}+g}{\gamma(1+\dfrac{\mu_{\rm r}}{k}\gamma)}\right)\tilde{H}_z(\alpha,0)e^{-\gamma lo} \qquad (1)\end{aligned}$$

where $\tilde{\tilde{\psi}}_{\rm i}$ is the 2-D FT of the potential functions representing the incident field in the absence of the metal, $\tilde{\tilde{\psi}}_{\rm i}, \gamma = \sqrt{\alpha^2+\beta^2}$ and α and β are, respectively, the Fourier variables associated with x and y, $k = \sqrt{j\omega\mu\sigma}$ and lo is the sensor liftoff distance. In (1), $\tilde{\tilde{\psi}}_i$ is a known quantity for a given inducer [4] and $\tilde{H}_z(\alpha,0)$ is the one-dimensional (1-D) FT of the normal component of the magnetic field at the crack opening just inside the crack, i.e., $H_z(x,0) = |Hz(x,z)|_{z=0}$. The solution of $\tilde{H}_z(x,0)$ can be sought by numerically treating a Laplacian boundary value problem representing the field inside the crack [5].

Having obtained $H_z(x,0)$ [5], one can use its 1-D FT, $\tilde{H}_z(\alpha,0)$, in (1) to obtain the potential function $\tilde{\tilde{\psi}}$ above the metal. A fast inverse 2-D FT algorithm is used to determine $\psi(x,y,z)$ from which the magnetic field (i.e., sensor output signal) everywhere above the metal can be determined.

The third term on the right-hand side of (1), $\tilde{\tilde{\psi}}_{\rm c}$, is the 2-D FT of the potential function $\psi_{\rm c}$ corresponding to the field perturbation, $\boldsymbol{H}_{\rm c}$, caused by the crack at the sensor position, i.e.,

$$\tilde{\tilde{\psi}}_{\rm c}(\alpha,\beta,lo) = \frac{\left(\frac{2\mu_{\rm r}}{k}+g\right)}{\gamma\left(1+\frac{\mu_{\rm r}}{k}\gamma\right)}\tilde{H}_z(\alpha,0)e^{-\gamma lo}. \qquad (2)$$

Note that

$$\tilde{\tilde{H}}_{{\rm c},x}(\alpha,\beta,lo) = -j\alpha\tilde{\tilde{\psi}}_{\rm c}(\alpha,\beta,lo) \qquad (3)$$

where $\tilde{\tilde{H}}_{{\rm c},x}(\alpha,\beta,lo)$ is the 2-D FT of x-component of $\boldsymbol{H}_{\rm c}$ at the sensor position, $H_{{\rm c},x}(x,y,lo)$. Assuming that the sensor is aligned in the x-direction, it is deduced from (2) and (3) that the nonzero value of lo has a 2-D low-pass filtering effect on the crack signal $(H_{{\rm c},x}(x,y,0))$ whose behavior is characterized by the liftoff filter function expressed by $G(\alpha,\beta,lo) = {\rm e}^{-\gamma lo}$ in the Fourier domain. As a result, this filtering effect tends to smear out any sharp variations in the crack signal. This phenomenon leads to significant errors when such blurred signals are inverted to crack shape by the inversion techniques commonly used for surface crack signals [7], [8].

To overcome the problem posed above, we propose a blind deconvolution algorithm for suppressing the liftoff effects on the crack signal. The algorithm estimates the liftoff distance and restores the surface crack signal using a conventional deconvolution procedure.

III. Restoration of Surface Crack Signal

From (2) and (3), the x-component of spatial magnetic field distribution on the surface of the metal, $H_{{\rm c},x}(x,y,0)$, could be restored by a deconvolution process from the corresponding blurred sensor output signal, $H_{{\rm c},x}(x,y,lo)$. This can be interpreted as a division operation in the frequency domain as follows:

$$\tilde{\tilde{H}}_{c,x}(\alpha,\beta,0) = \frac{\tilde{\tilde{H}}_{c,x}(\alpha,\beta,lo)}{G(\alpha,\beta,lo)}. \qquad (4)$$

Computation of (4) is not, however, straightforward as the value of lo in liftoff filter function G is not known. To overcome the problem, we start by assigning an initial value to lo. The correction of lo is then followed, using an iterative algorithm based on a blind deconvolution method. A comprehensive review of the blind deconvolution method together with classification of solutions has been presented in [9]. However, the solutions to these problems are very specific depending on the application and particularly the type of available *a priori* information. Here, the restoration of surface crack signal is carried out iteratively until lo becomes as close as possible to its true value. In other words, as *a priori* information, the algorithm employs the available closed-form expressions for the distribution of electromagnetic fields at the metal surface in the vicinity of cracks.

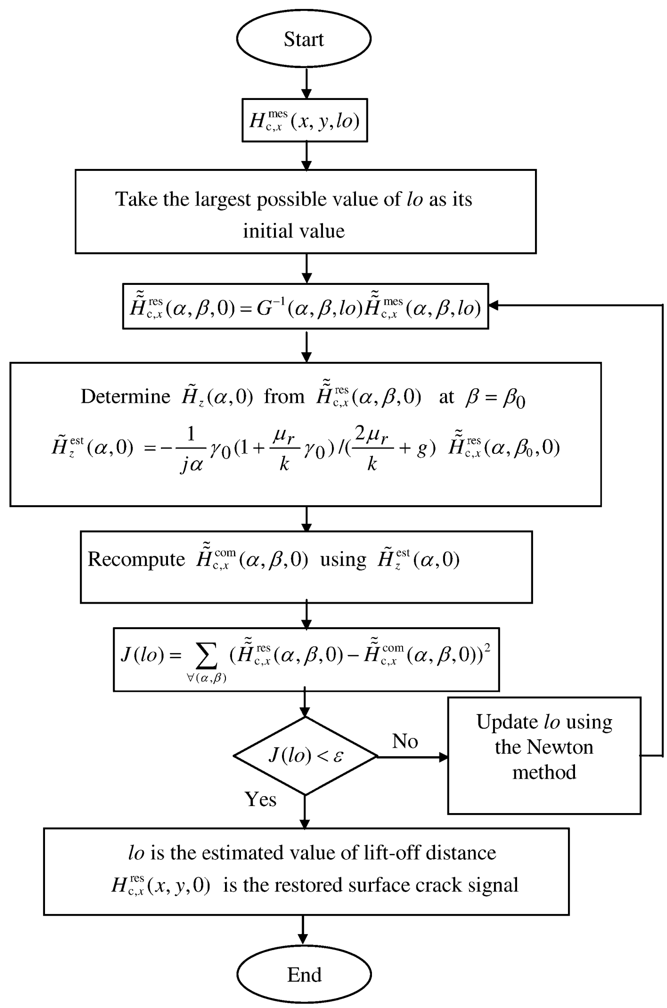

Fig. 2. Flowchart of the proposed blind deconvolution algorithm for estimating the unknown sensor liftoff distance and restoring surface crack signal.

The proposed algorithm is summarized in the flowchart shown in Fig. 2 and is described in the following steps.

a) Measure $H^{\text{mes}}_{c,x}(x,y,lo)$ by orienting the magnetic field sensor along the x-direction at an arbitrary distance, lo, above the metal surface. Although the movement of probe may cause variations in the value of lo, the algorithm will predict its average value.

b) Select the upper bound of the desired search region for finding liftoff distance and take it as the initial liftoff value.

c) For a given value of lo, follow the steps described below:

i) Using (4), restore the 2-D FT of the surface crack signal, $\tilde{\tilde{H}}^{\text{res}}_{c,x}(\alpha,\beta,0)$, from the the 2-D FT of the measured signal, $\tilde{\tilde{H}}^{\text{mes}}_{c,x}(\alpha,\beta,lo)$.

ii) Using (2) and (3), evaluate $\tilde{H}_z(\alpha,0)$ at the crack opening (i.e., $-l/2 \le x \le l/2$) for a constant value β_0 as follows:

$$\tilde{H}^{\text{est}}_z(\alpha,0) = -\frac{1}{j\alpha}\cdot \gamma_0\left(1+\frac{\mu_r}{k}\gamma_0\right)\Big/\left(\frac{2\mu_r}{k}+g\right)\tilde{\tilde{H}}^{\text{res}}_{c,x}(\alpha,\beta_0,0) \quad (5)$$

where $\gamma_0=\sqrt{\alpha^2+\beta_0^2}$. Note that the value of β_0 is selected arbitrarily and is retained unchanged during the restoration procedure. $\tilde{H}^{\text{est}}_z(\alpha,0)$ is a function of crack depth profile and will be used to estimate the surface crack signal without knowing the real depth profile. This is performed in the next step.

iii) Using $\tilde{H}^{\text{est}}_z(\alpha,0)$ in (2) and (3), recompute the 2-D FT of surface crack signal for all values of α and β as follows:

$$\tilde{\tilde{H}}^{\text{com}}_{c,x}(\alpha,\beta,0) = -j\alpha\frac{\left(\frac{2\mu_r}{k}+g\right)}{\gamma\left(1+\frac{\mu_r}{k}\gamma\right)}\tilde{H}^{\text{est}}_z(\alpha,0). \quad (6)$$

iv) Compute the square error, $J(lo)$, between the restored and computed values of 2-D FT of magnetic fields obtained in stages (i) and (iii), respectively, and take it as the cost function for estimating lo:

$$J(lo) = \sum_{\forall(\alpha,\beta)}\left(\tilde{\tilde{H}}^{\text{res}}_{c,x}(\alpha,\beta,0) - \tilde{\tilde{H}}^{\text{com}}_{c,x}(\alpha,\beta,0)\right)^2. \quad (7)$$

d) Check the termination condition $J(lo) < \varepsilon$ where ε is a predetermined small value. If the condition holds, go to step f).

e) Update the value of lo using the Newton method [10] for finding the global minimum of J and return to step c) to start a new iteration. The value of lo in the new $(k+1)$th iteration, lo_{k+1}, is determined as follows [10]:

$$lo_{k+1} = lo_k - \frac{lo_k - lo_{k-1}}{\frac{\partial}{\partial lo}J(lo_k) - \frac{\partial}{\partial lo}J(lo_{k-1})}\frac{\partial}{\partial lo}J(lo_k) \quad (8)$$

where lo_k and lo_{k-1} are, respectively, the values of lo in the present and last iterations.

f) The value of lo for which the cost function is minimized is the estimated value of the sensor liftoff. Also, the inverse FT of $\tilde{\tilde{H}}^{\text{res}}_{c,x}(\alpha,\beta,0)$ obtained at this liftoff value is the restored surface crack signal.

The convergence of the iterative procedure described above is proved in the Appendix.

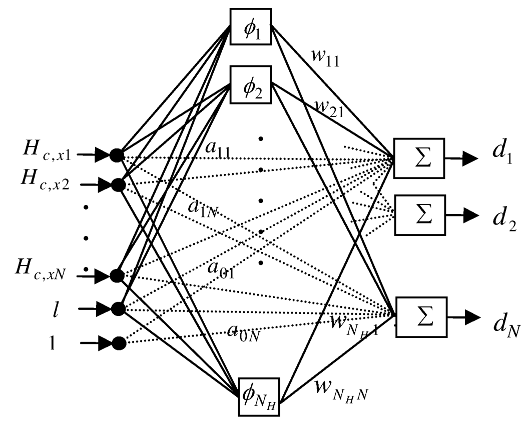

Fig. 3. Schematic of the wavelet network.

IV. Wavelet Network Inversion Model

The surface crack signals restored by the proposed algorithm will be used to estimate crack depth profile in an inversion

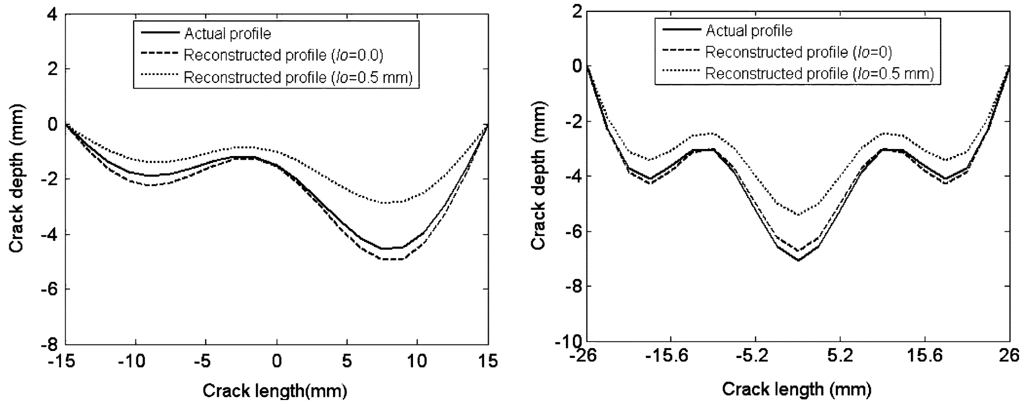

(a) (b)

Fig. 4. Actual and WN-reconstructed crack depth profiles using nonzero-liftoff and restored surface (zero-liftoff) crack signals. (a) Asymmetrical double-hump depth profile. (b) Symmetrical triple-hump depth profile.

process. We use a wavelet network to solve the inverse problem of crack depth profile identification [7].

To simplify the inversion process, without losing any generality, it is assumed that the crack opening is known and its length and depth lie between two limiting cases, i.e.,

$$l_{\min} \leq l \leq_{\max} \tag{9a}$$

$$d_{\min} \leq d(x) \leq d_{\max} \tag{9b}$$

where $l_{\min}$ and $l_{\max}$ are, respectively, the minimum and maximum values of expected crack length, and $d_{\min}$ and $d_{\max}$ denote, respectively, the minimum and maximum values of the deepest point in crack depth profile.

An appropriate database involving random generation of the crack depth profile is formed for network learning. The crack shape is approximated with N equidistance $(\Delta x = l/(N-1))$ points such that the nth point has depth of $d_n (n = 1, 2, \ldots, N)$ as shown in Fig. 1(b). After selection of N_2 suitable different crack shapes, new crack shapes are generated by assigning N_1 number of length values within the acceptable range to each crack depth profile [7]. It is worth noting that the crack length and direction in the ACFM technique can be obtained by performing a two-dimensional scan of the crack [3]. Thus, l is considered as *a priori* information and will be an input entry to the network.

After establishing the database, output signal of the magnetic field sensor at the surface of the metal is predicted for each crack entry in the database. To attain a good correlation between the crack depth profile and sensor output, the magnetic sensor axis is chosen to be parallel to the crack opening in order to measure the x-component of the magnetic field along the crack opening at a given distance y_{s} [7].

Also, the real part of the surface perturbed field caused by the crack, $H_{\mathrm{c},x}(x, y, 0)$, is used as the network input data. To attain this signal, the sensor output signal has been subtracted from its value in the absence of the crack. Since the presence of the noise in a practical measurement system is inevitable, white Gaussian noise is added to crack signals in database to improve the robustness of the network against noise.

The network structure is shown in Fig. 3. The proposed network has the following layers: an input layer consisting of $N + 1$ units, which receives discretized crack signal (i.e., $H_{\mathrm{c},x_1}, H_{\mathrm{c},x_2}, \ldots, H_{\mathrm{c},x_N}$) and crack length, l, a hidden layer of N_H neurons (wavelets), and an output layer consisting of N neurons, giving information about the discretized crack depth profile $(d_1, d_2, \ldots, d_N)$.

V. Results

Results of various simulation and experimental tests are presented here to assess the effect of liftoff removal procedure on the accuracy of crack sizing by the wavelet network method. For the training of the network, we assume $l_{\min} = 10$ mm, $l_{\max} = 140$ mm, $d_{\min} = 1$ mm, $d_{\max} = 10$ mm, $N = 10$, $N_H = 15$, $N_1 = 14$, and $N_2 = 100$. Also, white Gaussian noise with signal-to-noise ratio (S/N) of 25, 20 and 15 dB is added to crack signals in database. Due to the uncertainty in the value of sensor liftoff, the network is trained for surface crack signals.

A. Simulation Results

In order to demonstrate the accuracy of the proposed algorithm, two simulated results are presented. In these simulations, the ACFM probe scans two arbitrary shape cracks with two- [Fig. 4(a)] and three- [Fig. 4(b)] hump depth profiles and opening $g = 0.2$ mm. The specifications of the ACFM probe (Fig. 1) are: $w = 130$ mm, $s = 5$ mm, $t = 6$ mm, $L = 110$ mm, and $h = 15$ mm, $I_m = 1$ A and $f = 20$ kHz. We assume that the inducer is placed stationary above the metal surface while the sensor samples the magnetic field above an aluminum test block ($\mu_r = 1$ and $\sigma = 3.7 \times 10^7$ S/m).

To show the effect of sensor liftoff on the network response, surface crack signal is convolved with an appropriate liftoff filter function computed for the given value of liftoff. Fig. 5 shows the 2-D blurred and restored surface crack signals for the two cracks of Fig. 4(a) and (b) when $lo = 0.5$ mm. In these figures, the deleterious effect of liftoff distance on crack signals clearly is observed. For the purpose of crack sizing, the results associated with scanning along the crack opening at the distance of $y_s = 0.5$ mm are selected, Fig. 6(a) and (b). These results are used as input entries to the developed wavelet network, producing respective reconstructions of crack depth profiles. A

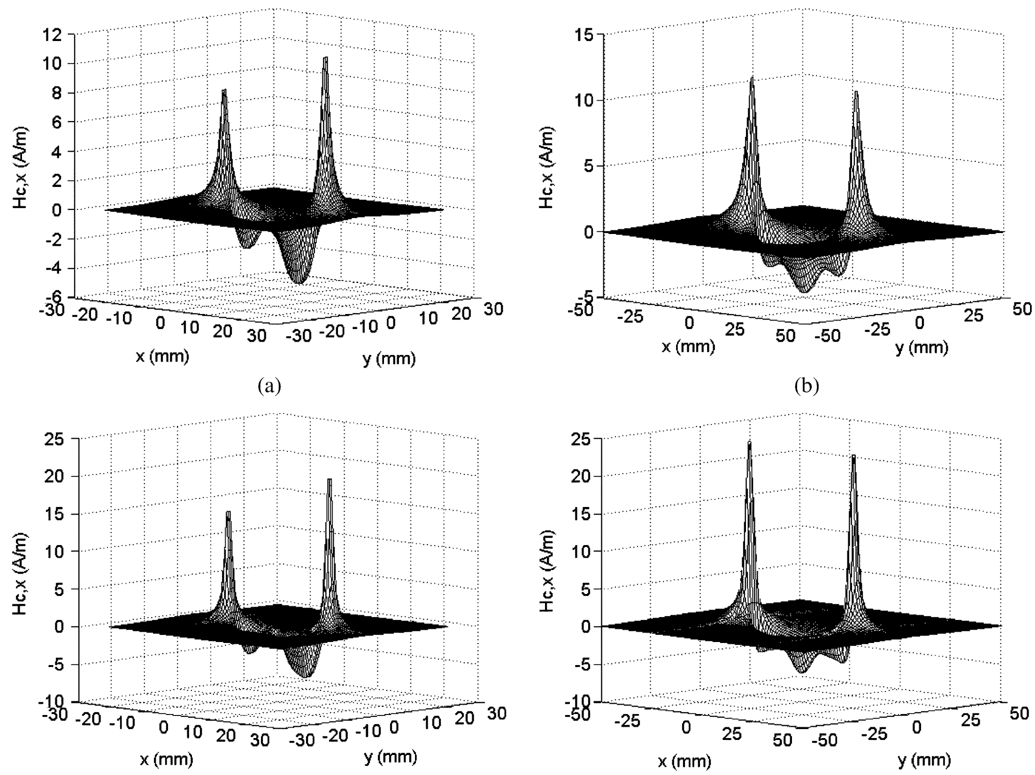

Fig. 5. 2-D variations of the real part of crack signals, $H_{c,x}$, when the sensor scans the metal surface at liftoff distance $lo = 0.5$ mm, together with their respective restored surface counterparts. (a) and (c) For asymmetrical double-hump depth profile. (b) and (d) For symmetrical triple-hump depth profile.

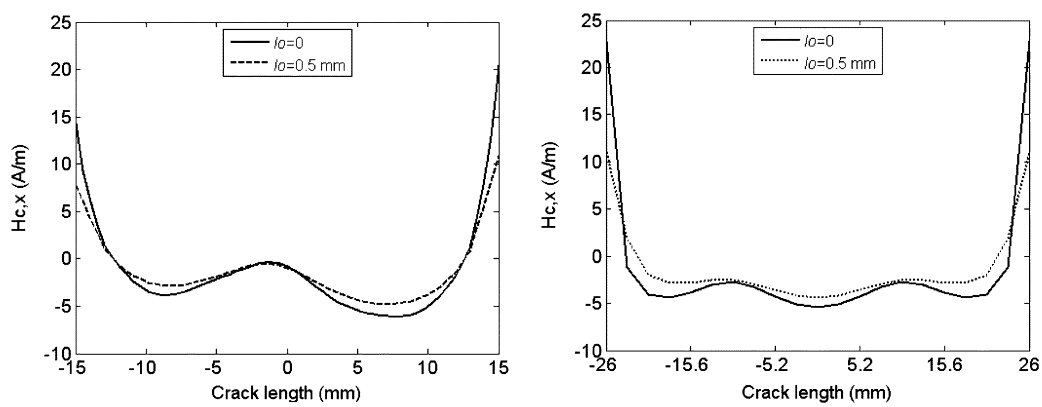

Fig. 6. 1-D variations of the real part of $H_{c,x}$, when scanning the cracks along $y_s = 0.5$ mm, together with their respective restored surface counterparts. (a) For asymmetrical double-hump depth profile. (b) For symmetrical triple-hump depth profile.

comparison of the actual and reconstructed results shown in Fig. 4(a) and (b) demonstrates the importance of the proposed algorithm. The results indicate that the new inversion methodology is capable of accurately reconstructing of various crack depth profiles at a nonzero liftoff distance. A quantitative comparison of these results can also be found in Table I where the root-mean-square deviation (RMSD) between the original crack depth profile, $d_n (n = 1, 2, \ldots, N)$, and its reconstructed counterpart, $\hat{d}_n (n = 1, 2, \ldots, N)$ in all cases are given:

$$\mathrm{RMSD} = \sqrt{\frac{\sum_{n=1}^{N} (d_n - \hat{d}_n)^2}{\sum_{n=1}^{N} d_n^2}} \times 100 \tag{10}$$

where d_n and $\hat{d}_n$, respectively, denote the nth point on the actual and WN predicted crack depth profile.

It is worth noting that with an initial guess of $lo = 1$ mm, the estimated values of liftoff for two- and three-hump cracks are found to be $lo = 0.49$ mm and 0.48 mm with estimation errors of 2% and 4%, respectively.

B. Experimental Results

To further examine the accuracy of the proposed algorithm, we present results of a typical ACFM inspection. During the inspection process, the inducer is placed stationary above the metal surface at a distance $h = 15$ mm while the sensor scans

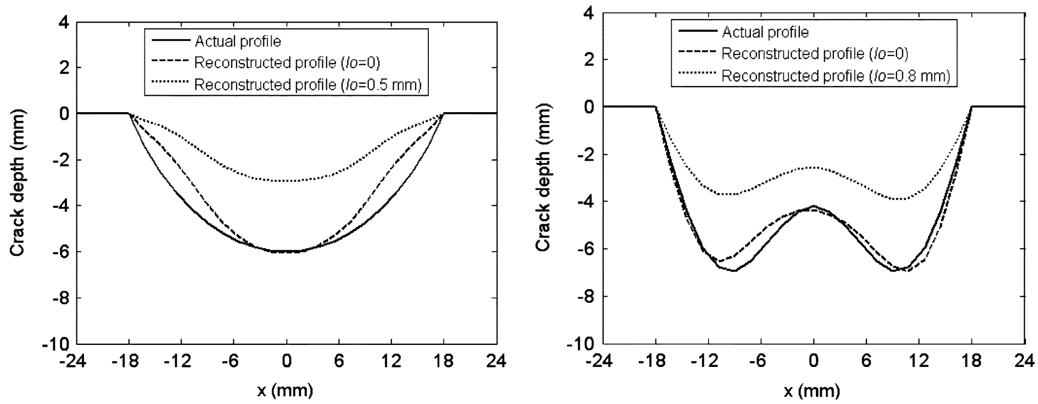

(a) (b)

Fig. 7. Depth profiles of two surface cracks together with their respective WN reconstructed results, using nonzero-liftoff and restored surface (zero-liftoff) crack signals. (a) Single-hump depth profile. (b) Symmetrical double-hump depth profile.

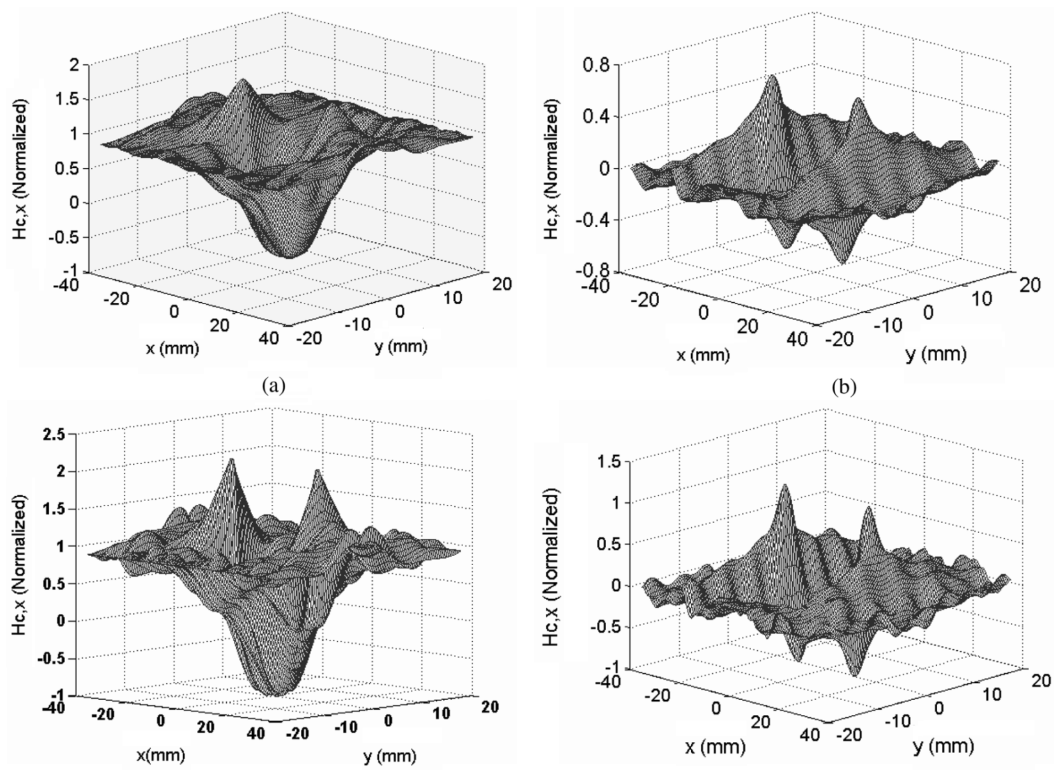

(a) (b) (c) (d)

Fig. 8. 2-D variations of the real part of crack signals, $H_{c,x}$, when the sensor scans the metal surface at nonzero liftoff distances, together with their respective restored surface counterparts. (a) and (c) For single-hump depth profile and $lo = 0.5$ mm. (b) and (d) For symmetrical double-hump depth profile and $lo = 0.8$ mm.

TABLE I
ERRORS IN THE PREDICTION OF CRACK DEPTH PROFILES SHOWN IN FIG. 4

lo (mm)	RMSD (blurred)	RMSD (restored)
Figure 4(a)		
0.3	14.8	11
0.5	35.2	10.3
0.7	51	9.8
Figure 4(b)		
0.3	22.7	2.2
0.5	35.3	3
0.7	45.8	2.8

the region under test. To obtain the crack signal, we subtract a background bias representing the sum of the incident field and the perturbed field due to the presence of metal. The value of bias is determined by scanning the specimen block in the crack-free region.

The ACFM probe specified in the previous section scans the surface of an aluminum slab ($\mu_r = 1$ and $\sigma = 3.7 \times 10^7$ S/m) of thickness $t_0 = 25$ mm, containing a surface crack with no predetermined geometrical depth profile. The sensor is a tiny pickup coil consisting of 12 turns of thin copper wire uniformly wound on a cylindrical glass holder with a length of 0.8 mm and radius of about 0.5 mm. Due to the small size of the sensor, it performs a point measurement of the magnetic field along the direction of its axis. The direction of magnetic sensor is duly selected to sample the x-component of the magnetic at the surface of the metal around the crack.

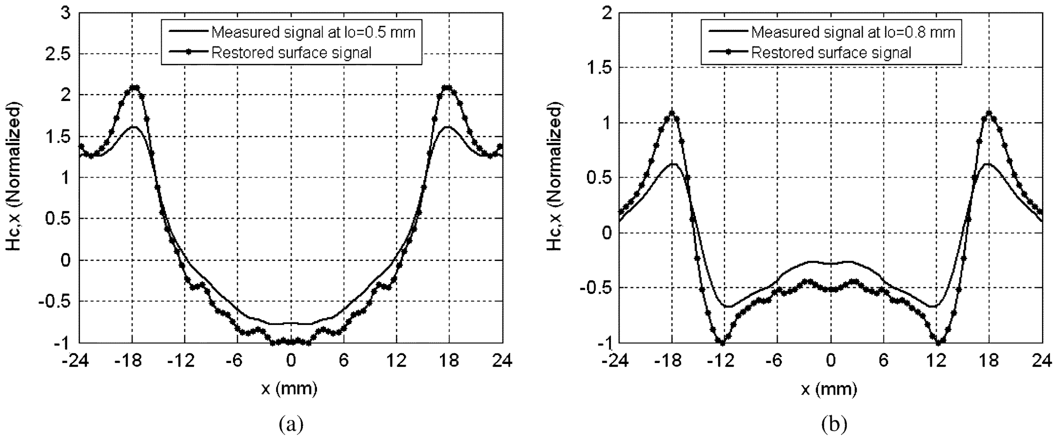

Fig. 9. 1-D variations of the real part of $H_{c,x}$, when scanning the cracks along $y_s = 0.5$ mm, together with their respective restored surface counterparts. (a) For single-hump depth profile. (b) For symmetrical double-hump depth profile.

TABLE II
ERRORS IN THE PREDICTION OF CRACK DEPTH PROFILES SHOWN IN FIG. 7

Crack	RMSD (blurred)	RMSD (restored)
Figure 7(a)	57.7	16.8
Figure 7(b)	43.5	7.4

Two surface cracks are manufactured using the electric discharge machinery (EDM) technique. They share the same length ($l = 36$ mm) and opening ($g = 0.2$ mm) but have various depth profiles, Fig. 7(a) and (b). The crack opening in each case starts at $x = -18$ mm and terminates at $x = 18$ mm. The results shown in Fig. 8(a) and (b) illustrate variations of $H_{c,x}$ for two cracks specified in Fig. 7(a) and (b), respectively, when the sensor performs 2-D scans of the metal surface at liftoff distances $lo = 0.5$ mm and $lo = 0.8$ mm, respectively. These results are used as input entries to the developed blind deconvolution algorithm, producing respective restoration of surface crack signals, Figs. 8(c) and (d). With an initial guess of $lo = 1$ mm, the estimated values of liftoff for the cases of Fig. 8(a) and (b) are found to be $lo = 0.54$ mm and $lo = 0.88$ mm with estimation errors of 8% and 10%, respectively.

For the purpose of crack sizing, the one-dimensional results associated with scanning along the crack opening at the distance of $y_s = 0.5$ mm are selected, Fig. 9(a) and (b). These results are used as input entries to the WN inversion algorithm to produce respective reconstructed crack depth profiles, Fig. 7(a) and (b). A comparison of the results shown in these figures demonstrates the accuracy of the proposed restoration algorithm. The RMSD values in both cases are given in Table II. As can be seen in this table, the value of RMSD in each case is not more than 16.8%.

VI. CONCLUSION

A blind deconvolution algorithm has been proposed for evaluating the unknown sensor liftoff and restoring the surface crack signal in the alternating-current field measurement (ACFM) technique. The algorithm uses the existing closed-form relations for electromagnetic field distributions around a crack as *a priori* information. The restoration of surface crack signal is carried out iteratively until the value of liftoff approaches its true value. To examine the accuracy of the proposed algorithm, a crack sizing wavelet-network inversion method is introduced which uses two input entries, namely, the blurred ACFM crack signal at an unknown liftoff distance and its respective restored crack signal at the metal surface. The accuracy of the proposed algorithm has been demonstrated by presenting several simulated and experimental results.

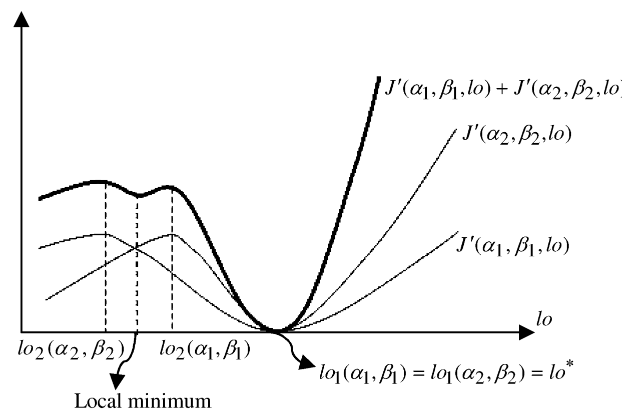

Fig. 10. Sum of two typical terms of the cost function J.

APPENDIX

Using (2)–(6), each term of the cost function (7), $J'(\alpha,\beta,lo)$, can be expanded as follows:

$$J'(\alpha,\beta,lo) = [A(e^{\gamma(lo-lo^*)} - e^{\gamma_0(lo-lo^*)})]^2 \tag{A1}$$

where

$$A = -j\alpha\frac{\left(\frac{2\mu_r}{k}+g\right)}{\gamma\left(1+\frac{\mu_r}{k}\gamma\right)}\tilde{H}_z(\alpha,0) \tag{A2}$$

and lo^* is the true value of the liftoff distance.

The stationary points of J' are determined by taking its first derivative with respect to lo and equating it to zero. These are given as follows:

$$lo_1 = lo^* \tag{A3}$$

$$lo_2 = \frac{\ln(\gamma/\gamma_0)}{\gamma_0 - \gamma} + lo^*. \tag{A4}$$

Since $J(lo^*) = J'(lo^*) = 0$, lo_1 becomes a global minimum point for both nonnegative functions J and J'. On the other hand, the negative sign of the second derivative of J' with respect to lo indicates that lo_2 is always a maximum point for J'. Since lo_2 is a function of α and β, one can expect several local minima for J. This is demonstrated in Fig. 10 where the sum of two typical terms of J, $J'(\alpha_1, \beta_1, lo)$ and $J'(\alpha_2, \beta_2, lo)$, are plotted.

To avoid local minima in the Newton search process [10], one must select a starting point that is greater than lo^*. This is due to the fact that lo_2, and likewise, any other possible local minimum points, are always smaller than lo_1 for all values of α and β, as seen in (A3) and (A4).

REFERENCES

[1] M. Lewis, D. H. Michael, M. C. Lugg, and R. Collins, “Thin-skin electromagnetic fields around surface-breaking cracks in metals,” *J. Appl. Phys.*, vol. 64, no. 8, pp. 3777–3784, Oct. 15, 1988.

[2] S. H. H. Sadeghi and D. Mirshekar-Syahkal, “Surface potential distributions due to eddy currents around long cracks in metals, induced by U-shaped current-carrying wires,” *IEEE Trans. Magn.*, vol. 27, no. 1, pp. 674–679, Jan. 1991.

[3] S. H. H. Sadeghi and D. Mirshekar-Syahkal, “Scattering of an induced surface electromagnetic field by fatigue cracks in ferromagnetic metals,” *IEEE Trans. Magn.*, vol. 28, no. 2, pp. 1008–1016, Mar. 1992.

[4] D. Mirshekar-Syahkal and R. F. Mostafavi, “Analysis technique for interaction of high-frequency rhombic inducer field with cracks in metals,” *IEEE Trans. Magn.*, vol. 33, no. 3, pp. 2291–2298, May 1997.

[5] M. Ravan, S. H. H. Sadeghi, and R. Moini, “Field distributions around arbitrary shape surface cracks in metals, induced by high frequency AC current—carrying wires of arbitrary shape,” *IEEE Trans. Magn*, vol. 42, no. 9, pp. 2208–2214, Sep. 2006.

[6] H. Fatehi, S. H. H. Sadeghi, R. Moini, and M. Fatehi, “Computation of electromagnetic field distribution due to an arbitrary shape exciter near multiplayer slab conductors,” *IEEE Trans. Magn.*, vol. 41, no. 3, pp. 1132–1136, Mar. 2005.

[7] M. Ravan, S. H. H. Sadeghi, and R. Moini, “Using a wavelet network for reconstruction of fatigue crack depth profile from AC field,” *NDT&E Int.*, vol. 40, no. 7, pp. 537–544, Oct. 2007.

[8] A. H. Salemi, S. H. H. Sadeghi, and R. Moini, “The effect of magnetic field sensor lift-off on SMFM crack signals,” in *Review of Progress in Quantitative Nondestructive Evaluation*. New York: Plenum, Aug. 2001, vol. 21, pp. 977–983.

[9] D. Kundur and D. Hatzinakos, “Blind image deconvolution,” *IEEE Signal. Process. Mag.*, vol. 13, no. 3, pp. 43–64, May 1996.

[10] P. E. Gill, W. Murray, and M. H. Wright, *Practical Optimization*. London, U.K.: Academic, 1981.

Manuscript received September 3, 2007; revised April 8, 2008. Corresponding author: S. H. H. Sadeghi (e-mail: sadeghi@aut.ac.ir).